Two-Dimensional and Three-Dimensional Fermi Surfaces of Superconducting $BaFe_2(As_{1-x}P_x)_2$ and Their Nesting Properties Revealed by Angle-Resolved Photoemission Spectroscopy

T. Yoshida,[1,2] I. Nishi,[1] S. Ideta,[1] A. Fujimori,[1,2] M. Kubota,[3] K. Ono,[3] S. Kasahara,[4,5] T. Shibauchi,[5] T. Terashima,[4] Y. Matsuda,[5] H. Ikeda,[2,5] and R. Arita[2,6]

[1]*Department of Physics, University of Tokyo, Bunkyo-ku, Tokyo 113-0033, Japan*
[2]*Transformative Research-Project on Iron Pnictides (TRIP), JST, Chiyoda, Tokyo 102-0075, Japan*
[3]*KEK, Photon Factory, Tsukuba, Ibaraki 305-0801, Japan*
[4]*Research Center for Low Temperature and Materials Sciences, Kyoto University, Kyoto 606-8502, Japan*
[5]*Department of Physics, Kyoto University, Kyoto 606-8502, Japan*
[6]*Department of Applied Physics, University of Tokyo, Bunkyo-ku, Tokyo 113-8561, Japan*

(Received 12 August 2010; published 18 March 2011)

We have studied the three-dimensional shapes of the Fermi surfaces (FSs) of $BaFe_2(As_{1-x}P_x)_2$ ($x = 0.38$), where superconductivity is induced by isovalent P substitution and by angle-resolved photoemission spectroscopy. Moderately strong electron mass enhancement has been identified for both the electron and hole FSs. Among two observed hole FSs, the nearly two-dimensional one shows good nesting with the outer two-dimensional electron FS, but its orbital character is different from the outer electron FS. The three-dimensional hole FS shows poor nesting with the electron FSs. The present results suggest that the three dimensionality and the difference in the orbital character weaken FS nesting while partial nesting among the outer electron FSs of d_{xy} character and/or that within the three-dimensional hole FS becomes dominant, which may lead to the nodal superconductivity.

DOI: 10.1103/PhysRevLett.106.117001 PACS numbers: 74.25.Jb, 71.18.+y, 74.70.−b, 79.60.−i

Most of experimental results on the iron-pnictide superconductors have so far indicated that the superconducting gap opens on the entire Fermi surfaces [1,2], most likely a $s\pm$-wave gap, in contrast to the d-wave superconducting gap in the high-T_c cuprate superconductors. However, recent penetration depth, thermal conductivity [3], and NMR [4] studies of $BaFe_2(As_{1-x}P_x)_2$ [5] show signatures of a superconducting gap with a line node. In this system, the substitution of P for As suppresses magnetic order without changing the number of Fe $3d$ electrons and induces superconductivity with a maximum $T_c \sim 30$ K at $x \sim 0.3$. According to theories of spin-fluctuation-mediated superconductivity, line nodes may appear when the pnictogen height becomes small [6,7], due to changes in nesting conditions caused by the disappearance of a hole Fermi surface (FS) of d_{xy} character around the zone center. (Here, the x and y axes point towards nearest neighbor Fe atoms.)

The importance of FS nesting for the superconductivity has been pointed out in early studies on $Ba_{1-x}K_xFe_2As_2$ by angle-resolved photoemission spectroscopy (ARPES) [1,2] based on models with 2D electronic structure. For the family of the $BaFe_2As_2$ system, however, strong three dimensionality in FSs has been identified by the band-structure calculation [8] and confirmed by ARPES studies [9,10]. Because the P substitution in $BaFe_2(As_{1-x}P_x)_2$ reduces the c axis length as well as pnictogen height and increases the interlayer hopping, band-structure calculation predicts that the shapes of hole FSs become more three dimensional with P substitution [5,11,12]. Therefore, it is crucial to reveal the three-dimensional electronic structure of the $BaFe_2(As_{1-x}P_x)_2$ superconductor in order to elucidate the relationship between FS nesting, superconductivity, and gap symmetry. de Haas–van Alphen (dHvA) measurements [12] in a wide substitution range ($0.41 < x < 1$) have indicated a shrinkage of the electron FSs compared to the band-structure calculation as one approaches the optimal composition from the end material $BaFe_2P_2$ ($x = 1$) Also, significant electron mass renormalization has been observed there, which is reminiscent of heavy fermion superconductors.

In the present study, we have studied the three-dimensional shapes of the FSs near the optimal composition ($x = 0.38$) by performing ARPES measurements. Using tunable photon energies of synchrotron radiation, we have observed FSs predicted by band-structure calculation in the three-dimensional momentum space. Also, we have observed electron mass renormalization for each FS, quantitatively consistent with the dHvA results [12]. Based on the obtained FSs, we shall discuss the FS nesting properties in the three-dimensional momentum space and their implication for the nodal superconductivity.

High-quality single crystals of $BaFe_2(As_{1-x}P_x)_2$ with $x = 0.38$ ($T_c = 28$ K) were grown as described elsewhere [5]. ARPES measurements were carried out at BL-28A of Photon Factory using circularly polarized light. A Scienta SES-2002 analyzer was used with a total energy resolution of $\sim$15 meV and a momentum resolution of $\sim 0.02\pi/a$. In-plane (k_X, k_Y) and out-of-plane electron momenta (k_z) are expressed in units of π/a and $2\pi/c$, respectively,

where $a = 3.92$ Å and $c = 12.8$ Å are the in-plane and the out-of-plane lattice constants. Here, the tetragonal unit cell axes are defined as X, Y, and z. The crystals were cleaved *in situ* at $T = 10$ K in an ultrahigh vacuum of $\sim 5 \times 10^{-11}$ Torr. Calibration of the Fermi level (E_F) of the samples was achieved by referring to that of gold. Our data are compared with a band-structure calculation performed using a WIEN2K package [13].

FS mapping in the k_X-k_Y plane is shown in Figs. 1(a) and 1(b). By assuming an inner potential $V_0 = 13.5$ eV, Figs. 1(a) and 1(b) approximately correspond to the k_X-k_Y planes including the Z and the Γ point, respectively. We have observed at least two hole FSs around the center of the Brillouin zone (BZ) and two electron FSs around the corner of the BZ. One can clearly see a small diameter of the hole FSs around the Γ point compared to those around the Z point, suggesting strong three dimensionality of the FSs. Band dispersions corresponding to cuts in Figs. 1(a) and 1(b) are illustrated in Figs. 1(c)–1(f). In particular, for the electron band dispersions around the X point, two sheets of FSs have been observed as shown in Figs. 1(a) and 1(d), consistent with the band-structure calculation.

In order to further investigate the three-dimensional electronic structure, intensity mapping in the $k_\parallel$-k_z plane was performed by changing the photon energy as shown in Fig. 2. The direction of $k_\parallel$ is the same as the cuts in Fig. 1. Intensity maps in Figs. 2(a) and 2(b) illustrate the cross sections of the Fermi surfaces by the $k_\parallel$-k_z plane around the center and the corner of the BZ, respectively. Note that the intensity asymmetry observed with respect to the $k_\parallel = 0$ line is due to photoemission matrix elements. By symmetrizing the plots in Figs. 2(a) and 2(b), we have obtained the experimental FSs as shown in Fig. 2(c). For comparison, results of band-structure calculation for $x = 0.4$ and 0.6 are shown in Figs. 2(d) and 2(e), respectively. Here, the band-structure calculation has been performed for $BaFe_2As_2$ with the experimentally determined lattice constants and pnictogen height [5] for $BaFe_2(As_{1-x}P_x)_2$ with $x = 0.4$ and 0.6 in order to look into the effects of the pnictogen height. As illustrated in the figure, we denote the hole FSs around the center of the BZ by α, β, and γ, respectively, and the outer and inner electron FSs around the corner of the BZ are denoted by δ and ϵ, respectively. Note that the β and γ FSs intersect each other [14].

As shown in Fig. 2(c), the inner electron FS ϵ exhibits warping qualitatively consistent with the calculation. Judging from this consistency, one can conclude that the inner and outer electron FSs have $d_{xz/yz}$ and d_{xy} character, respectively. Correspondences between the observed hole FSs and the calculation are not straightforward because we have observed only two hole FSs as shown in Figs. 1 and 2(a) while the band-structure calculation predicts three hole FSs. As for the inner hole FS around the Γ point, a very recent ARPES result on the similar system $EuFe_2(As_{1-x}P_x)_2$ has revealed that this FS has $d_{xz/yz}$ orbital character [15]. Also, the matrix element of the d_{xy} orbital around the Γ point should be much smaller than

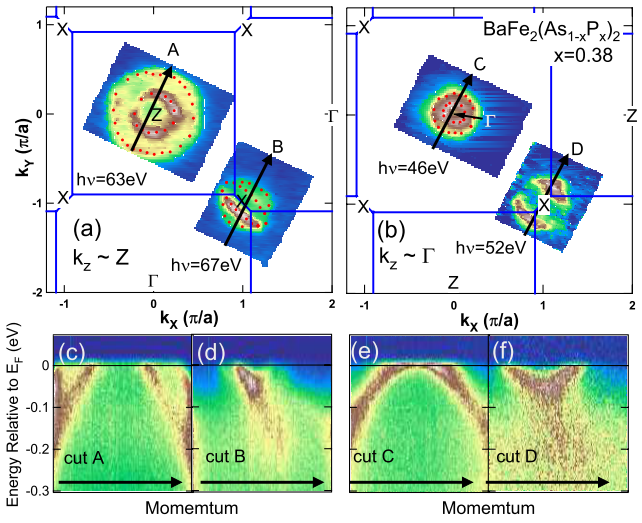

FIG. 1 (color online). Fermi surfaces and band dispersions of $BaFe(As_{1-x}P_x)_2$ ($x = 0.38$) observed by ARPES. (a),(b) ARPES intensity at E_F mapped in the k_X-k_Y plane taken at several photon energies. The Brillouin zone boundary is shown by blue lines. Red dots indicate k_F positions determined by the peak positions of momentum distribution curves. (c)–(f) Band dispersion corresponding to the cuts in (a) and (b).

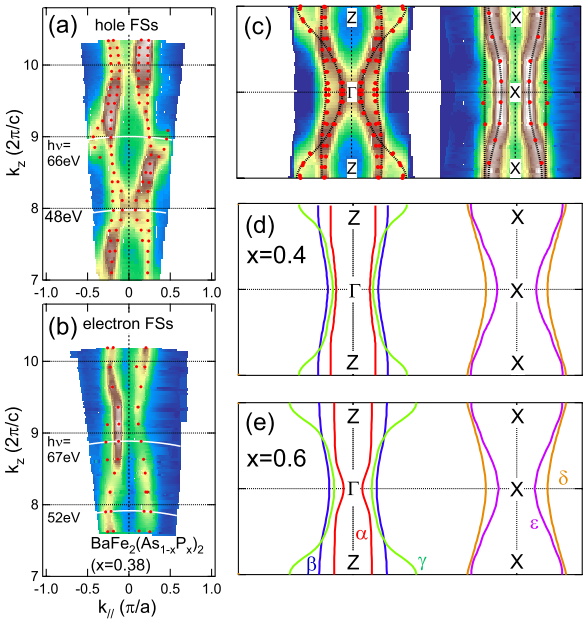

FIG. 2 (color online). Fermi surface mapping in the $k_\parallel$-k_z plane obtained by changing the photon energy. (a) Hole Fermi surfaces around the center of the Brillouin zone (BZ). (b) Electron Fermi surfaces around the corner of the BZ. The directions of $k_\parallel$ are shown in Fig. 1. (c) Fermi surfaces obtained by symmetrizing the plots in (a) and (b). (d),(e) Band-structure calculation for $x = 0.4$ and 0.6.

those of the $d_{xz/yz}$ orbital [16]. Therefore, this FS cannot be the α FS which has nearly pure d_{xy} orbital character but the three-dimensional γ FS with $d_{xz/yz}$ orbital character. As for the observed nearly two-dimensional hole FS, if we assume that this FS is the α FS, the energy level of the d_{xy} band should be much higher than that of the $d_{xz/yz}$ band at the Γ point, which contradicts the general prediction of band-structure calculation. Therefore, the observed nearly two-dimensional hole FS is assigned to the β FS of $d_{xz/yz}$ orbital character. In Fig. 2(c), we illustrate the β and γ FSs according to our observation. We could not identify the α FS probably because the spectral intensity is too weak and/or the band is nearly degenerate with the β and γ bands.

In the dHvA measurements, the effective mass of the δ electron FS increases with decreasing x down to $x \sim 0.4$, similar to the quantum critical behavior of heavy fermion systems [12]. The present ARPES data enable us to directly determine the effective masses for each FS, by fitting a parabolic band to the band dispersion as shown in Fig. 3. The effective masses determined by ARPES as well as those derived from the band-structure calculation are summarized in Table I. For the δ and ϵ FSs, the effective mass ratios m^*/m_e, where m_e is the free electron mass, are estimated to be 2.8 and 2.0, respectively. Particularly, the value for the δ FS is nearly the same as that of the dHvA result for $x = 0.41$ ($m^*/m_e \sim 3.3$). The mass enhancement factor m^*/m_b, where m_b is the band mass obtained by the band-structure calculation, varies from 1.3–3.9 for these FSs. As a whole, these values are comparable to or larger than those for the end members, $SrFe_2P_2$ ($m^*/m_b \sim$ 1.3–2.1) and $CaFe_2P_2$, ($m^*/m_b \sim 1.5$) [17,18]. Thus, the observed mass enhancement factors indicate moderately strong electron correlation effects and may be related to the proximity to the quantum critical point.

We have determined the three-dimensional volumes of the FSs as listed in Table I. To estimate the FS volume,

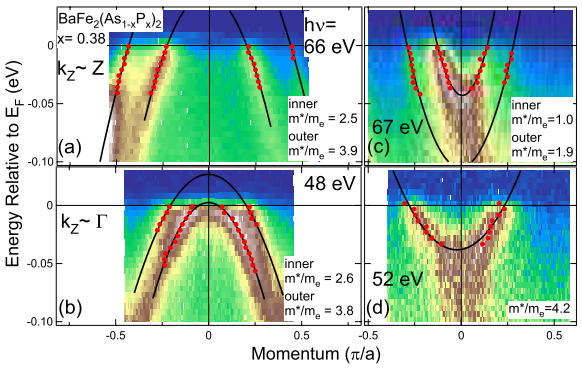

FIG. 3 (color online). Band dispersions around the BZ center [(a),(b)] and the BZ corner [(c),(d)] corresponding to the cuts in Figs. 2(a) and 2(b). Filled circles indicate peak positions of the momentum distribution curves obtained by taking second derivatives. Mass renormalization for each band is obtained by fitting to parabolic dispersions.

TABLE I. Fermi surface volumes and effective masses of $BaFe_2(As_{1-x}P_x)_2$ ($x = 0.38$) determined by ARPES. m_b/m_e's are obtained by band-structure calculation for $x = 0.4$. The cross-section areas of the FSs and the three-dimensional FS volumes are expressed in percent of the area defined by $(2\pi/a)^2$ and the volume of the 3D BZ, respectively. For the hole FSs (β and γ), m^*/m_e's determined from Fig. 3 are listed because the hole FSs are nearly isotropic in the k_X-k_Y plane. m^*/m_e's for the anisotropic FSs (δ, ϵ) are determined assuming $m^* = \sqrt{m_x^* m_y^*}$, where m_x^* and m_y^* are masses in the two orthogonal axes.

FS	3D volume	k_z	Cross-section area	m^*/m_e	m_b/m_e	m^*/m_b
β	3.9	Γ	3.9	3.8	2.1	1.8
		Z	3.8	2.5	1.3	1.9
γ	6.0	Γ	1.0	2.6	1.2	2.2
		Z	16.3	3.9	2.9	1.3
δ	5.3	X	5.3	2.8	0.72	3.9
ϵ	3.4	X	3.0	2.0	1.1	1.8

we have taken into account the warping of the FSs along the k_z direction. The volume of the electron FSs δ (5.3% of BZ) and ϵ (3.4% of BZ) are in good agreement with those for $x = 0.4$ obtained by the dHvA measurements, ~6% and ~3%, respectively [12]. The experimentally determined electron FSs are much smaller than those predicted by the band-structure calculation, as clearly seen in Figs. 2(c)–2(e). As for the hole FSs, the γ FS shows strong shrinkage around the Γ point compared to the calculation, while that around the Z point has almost the same diameter as the theoretical prediction. The total electron and hole count from the observed FSs yields holes of 1.2% of the BZ volume, indicating nearly compensated carriers although contribution from the α hole FS is not included. To precisely determine the carrier number, further investigation is necessary to detect the α band.

Since FS nesting between electron and hole FSs has been discussed as a necessary ingredient for the superconductivity in the previous studies [1,2], we shall discuss the nesting properties of the FSs in three-dimensional momentum space. The shapes of the observed FSs are reproduced in Figs. 4(a) and 4(b). Here, hole FSs shifted by the antiferromagnetic wave vector $(\pi/a, \pi/a, 2\pi/c)$ of $BaFe_2As_2$ [19] are overlaid as dashed curves in Fig. 4(b). In a similar manner, the hole FSs are shifted by an in-plane vector $(\pi/a, \pi/a, 0)$ in Fig. 4(a). Note that the shifts by both vectors are equivalent in nesting conditions because the interval between two adjacent X points in the k_z direction is $2\pi/c$.

According to the spin-fluctuation mechanism of superconductivity [6,7], when a hole FS which has d_{xy} orbital character becomes absent, the fully gapped $s \pm$-wave superconducting state becomes unstable and the nodal

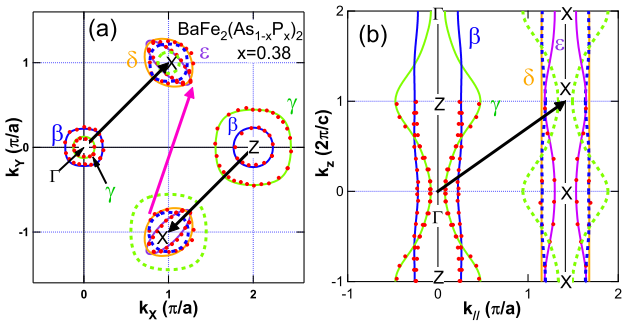

FIG. 4 (color online). FSs determined by ARPES in k_X-k_Y plane (a) and $k_z - k_{\|}$ plane (b). Dotted lines are hole FSs shifted by the antifferomagnetic vector (black arrows). Partial nesting between the neighboring δ FSs is indicated by a pink arrow.

s-wave or d-wave superconductivity is realized. This is because, in the spin susceptibility, the structure which arises from the partial nesting between the neighboring electron pockets of d_{xy} orbital becomes dominant.

Since we could not observe the α hole FS of d_{xy} orbital character, we shall discuss the nesting properties of other FSs. As shown in Fig. 4, the size of the β hole FS is nearly the same as that of the δ electron FS and both FSs have nearly cylindrical shapes, implying good nesting. However, these FSs have different orbital character: $d_{xz/yz}$ for the β FS and d_{xy} for the δ FS. Hence, the β-δ nesting may have small contribution to the spin susceptibility. The γ FS shows strong warping and therefore its nesting with the electron FSs is poor. Furthermore, the γ FS has $d_{3z^2-r^2}$ orbital character around the Z point, while $d_{3z^2-r^2}$ orbital character is almost absent in the electron FSs. To summarize, the contribution to the spin susceptibility from γ-ϵ nesting becomes small due to the orbital character and the three-dimensionality of the γ FS.

On the other hand, partial nesting between the neighboring δ electron FSs of d_{xy} orbital character persists, as indicated by the wave vector at the center of Fig. 4(a). Because interband scattering between the electron and hole FSs is reduced as mentioned above, the δ-δ partial nesting may give a dominant contribution to the spin susceptibility [6], which tends to change the sign of the gap between these pockets. That is, the three dimensionality of the γ FS and the difference of the orbital character between the hole and electron FSs suppress the fully gapped $s\pm$ pairing, leading to the nodal superconductivity.

An alternative scenario for the nodal superconductivity is an appearance of horizontal nodes, which is likely to be realized in the presence of warped hole FSs [20,21]. In fact, in the overdoped region of the electron-doped system $Ba(Fe_{1-x}Co_x)_2As_2$, which has strongly three-dimensional hole FSs [9,10], it has been pointed out that nodes occur in the Fermi surface that dominate c-axis conduction [22]. Possibly, the nodes result from partial nesting within the γ FS. If this scenario can be applied to the present system, the strongly three-dimensional γ FS may have horizontal nodes. This should be clarified in future studies.

In conclusion, we have experimentally determined the Fermi surfaces of $BaFe_2(As_{1-x}P_x)_2$ ($x = 0.38$) and found that the γ hole FS has highly three-dimensional shape, while the β hole FS is nearly two dimensional. We have discussed nesting conditions for the observed FSs. As a result of the poor nesting between the electron and hole FSs, the partial nesting between the δ FSs and/or that within the γ FSs becomes dominant. According to the spin-fluctuation mechanism [6], the partial nesting tends to change the sign of the gap between the nested FSs and thus the nodes in the superconducting gap on the hole FSs and/or the γ FS are likely to be realized. The present results give strong constraint on the theory of paring mechanism and imply the importance of the three-dimensional FSs in the nodal superconductivity.

We are grateful to K. Nakamura, T. Shimojima, W. Malaeb, K. Kuroki, and S. Shin for informative discussions. This work was supported by Grant-in-Aid for Scientific Research on Innovative Area "Materials Design through Computics: Complex Correlation and Non-Equilibrium Dynamics" from MEXT and the Japan-China-Korea A3 Foresight Program from the Japan Society for the Promotion of Science. Experiment at Photon Factory was approved by the Photon Factory Program Advisory Committee (Proposal No. 2009S2-005).

[1] H. Ding *et al.*, Europhys. Lett. **83**, 47 001 (2008).
[2] K. Terashima *et al.*, Proc. Natl. Acad. Sci. U.S.A. **106**, 7330 (2009).
[3] K. Hashimoto *et al.*, Phys. Rev. B **81**, 220501 (2010).
[4] Y. Nakai *et al.*, Phys. Rev. B **81**, 020503 (2010).
[5] S. Kasahara *et al.*, Phys. Rev. B **81**, 184519 (2010).
[6] K. Kuroki *et al.*, Phys. Rev. B **79**, 224511 (2009).
[7] H. Ikeda, R. Arita, and J. Kuneš, Phys. Rev. B **81**, 054502 (2010).
[8] D. J. Singh, Phys. Rev. B **78**, 094511 (2008).
[9] P. Vilmercati *et al.*, Phys. Rev. B **79**, 220503 (2009).
[10] W. Malaeb *et al.*, J. Phys. Soc. Jpn. **78**, 123706 (2009).
[11] J. G. Analytis *et al.*, Phys. Rev. Lett. **105**, 207004 (2010).
[12] H. Shishido *et al.*, Phys. Rev. Lett. **104**, 057008 (2010).
[13] P. Blaha *et al.*, WIEN2K, edited by K. Schwarz, Technische Universität Wien, Austria, 2001.
[14] Strictly speaking, the β and γ FSs show splitting at the cross section of the FSs due to spin-orbit interaction.
[15] S. Thirupathaiah *et al.*, arXiv:1007.5205.
[16] Y. Zhang *et al.*, arXiv:0904.4022v2.
[17] J. G. Analytis *et al.*, Phys. Rev. Lett. **103**, 076401 (2009).
[18] A. I. Coldea *et al.*, Phys. Rev. Lett. **103**, 026404 (2009).
[19] Q. Huang *et al.*, Phys. Rev. Lett. **101**, 257003 (2008).
[20] S. Graser *et al.*, Phys. Rev. B **81**, 214503 (2010).
[21] K. Suzuki, H. Usui, and K. Kuroki, J. Phys. Soc. Jpn. **80**, 013710 (2011).
[22] J.-P. Reid *et al.*, Phys. Rev. B **82**, 064501 (2010).